Direct Imaging of Radiation Sensitive Organic Polymer-Based Nanocrystals at Sub-Ångström Resolution

Elvio Carlino *, Antonietta Taurino, Dritan Hasa, Dejan-Krešimir Bučar, Maurizio Polentarutti, Lidia Esther Chincilla, Jose Juan Calvino Gamez

Posted Date: 22 April 2024

doi: 10.20944/preprints202404.1348.v1

Keywords: Radiation damage; Polymers; soft matter; HoloTEM; atomic Resolution Imaging; in-line Holography; HRTEM

 doi:10.20944/preprints202404.1348.v1

Article

Direct Imaging of Radiation Sensitive Organic Polymer-Based Nanocrystals at Sub-Ångström Resolution

Elvio Carlino [1,*], Antonietta Taurino [2], Dritan Hasa [3], Dejan-Krešimir Bučar [4], Maurizio Polentarutti [5], Lidia E. Chinchilla [6] and Josè J. Calvino Gamez [6]

[1] Istituto di Cristallografia del Consiglio Nazionale delle Ricerche (IC-CNR); Bari - Italy
[2] Istituto per la Microelettronica e i Microsistemi del Consiglio Nazionale delle Ricerche (IMM-CNR); Lecce – Italy
[3] Department of Chemical and Pharmaceutical Sciences University of Trieste; Trieste - Italy
[4] Department of Chemistry, University College London; London – United Kingdom
[5] Elettra-Sincrotrone Trieste; Basovizza (Trieste) - Italy
[6] Departamento de Ciencia de los Materiales, Ingeniería Metalúrgica y Química Inorgánica, Facultad de Ciencias, Universidad de Cádiz; Puerto Real (Cádiz) - Spain
* Correspondence: elvio.carlino@cnr.it

Abstract: Seeing atomic configuration of single organic nanoparticles at sub-Å spatial resolution by transmission electron microscopy has been so far prevented by the high sensitivity of soft matter to radiation damage. The difficulty is related to the need to irradiate the particle with a total dose of few electrons/Å^2, not compatible with the electron beam density necessary to search the low-contrast nanoparticle, to control its drift, to finely adjust the electro-optical conditions and particle orientation, and to finally acquire an effective atomic resolution image. On the other hand, the capability to study individual pristine nanoparticles, such as proteins, active pharmaceutical ingredients, and polymers, with peculiar sensitivity to the variation of the local structure, defects, and strain, would provide advancements in many fields, including materials science, medicine, biology, and pharmacology. Here we report direct sub-ångström resolution imaging at room temperature of pristine unstained crystalline polymer-based nanoparticles. This result is obtained by combining low-dose in-line electron holography and phase-contrast imaging on state-of-the-art equipment, providing an effective tool for the quantitative sub-angstrom imaging of soft matter.

Keywords: radiation damage; polymers; soft matter; HoloTEM; atomic resolution imaging; in-line holography; HRTEM

1. Introduction

Transmission electron microscopy (TEM) methods have been extremely successful for the improvement of our understanding of structural, electromagnetic, and chemical properties of matter, pushing the development of physics, materials science and chemistry [1–3]. Richard Feynman stated in his famous lecture "Plenty of room at the bottom" in 1959: "*It would be very easy to make an analysis of any complicated chemical structure; all one would have to do would be to look at it and see where the atoms are. The only trouble is that the electron microscope is one hundred times too poor… I put this out as a challenge: Is there no way to make the electron microscope more powerful?*" [4]. Since then, research in electron microscopy, both on the technological and methodological sides, focused on overcoming the limitations to the spatial resolution power of the electron microscope [5–7] with the aim to enable the highest resolution and accuracy in the understanding of the matter at the atomic level, for a conscious advance in a wide variety of fields of scientific and industrial relevance [1–3]. Nowadays, sub-ångström resolution is achievable by TEM and Scanning TEM (STEM) imaging methodologies, owing mainly to the development of spherical aberration correctors [8], and high-coherence and high-brilliance field emission sources [9]. Furthermore, the recent progress of direct conversion electron

 doi:10.20944/preprints202404.1348.v1

detectors enables atomic resolution imaging with unsurpassed signal-to-noise ratio and acquisition speed [10]. Unfortunately, however, High Resolution TEM (HRTEM) imaging of soft matter at sub-ångström resolution remains practically impossible [11–13] because of the severe and, so far, unavoidable specimen radiation damage occurring during the experiments [14]. Therefore, the biggest challenges in the development of TEM/STEM imaging and spectroscopies continue to be related to radiation damage, which is caused by the high density of electrons targeting the specimen [15]. For typical HRTEM imaging of inorganic specimens, a density of electrons, ρ, of some thousands of $e^-/Å^2$ or more, is delivered [16] while the study of organic matter requires extremely small electron doses to avoid structural damage. As a conservative rule of thumb, Henderson reports that, even at cryogenic temperature, the electron density delivered to the biologic specimen should not exceed 5 $e^-/Å^2$ at liquid nitrogen temperature and 20 $e^-/Å^2$ at liquid helium temperature [17], which are orders of magnitude lower than those currently applied for HRTEM imaging of single particle inorganic materials, like metals or semiconductors, which are relatively robust to radiation damage. Furthermore, the higher is the spatial resolution to be achieved and the higher is the dose of electrons necessary for effective imaging [18]. A successful high spatial resolution imaging experiment should answer our need to know where atoms in the structure (and which atoms) are but also, for example, if the bonds are locally strained or the structure is affected by a defect, as the properties of a material depend not only on the structure, but they are largely governed by strain and defects [19]. The steps necessary for effective HRTEM imaging experiment of single nanoparticles, are numerous and mainly consist in finding on the TEM grid the nanoparticle well oriented along a zone axis, waiting until the drift of the specimen holder stops, accurately fine tuning the electron-optical conditions on the area of interest, namely fine focusing and illumination convergence angle adjustment, (this latter step is mandatory to properly simulate the image to extract all the information encoded in the frame) and finally acquiring a high signal-to-noise HRTEM image [2]. All these steps must be performed without damaging the nanoparticle structure and must be repeated for a number of nanoparticles high enough to have a statistical significance in addressing quantitatively the specimen properties.

This is why sub-ångström HRTEM imaging of soft matter has not been reported so far in the literature despite several attempts [12,13]. Among soft matter, polymers are an example of extremely radiation sensitive material because electron densities lower than $0.2e^-/Å^2$ should be mandatory for imaging at 1Å resolution [18]. At these values of ρ, even the use of the most advanced high sensitivity direct conversion cameras results in images with faint contrast, which are practically useless for quantitative measurements of the specimen properties. Furthermore, all the steps necessary before the acquisition of the HRTEM image might have already damaged the particle. Examples of recent literature dealing with HRTEM on radiation sensitive materials report the experimental difficulties to achieve effective imaging experiments even when they do not tackle the most sensitive case of small nanoparticles. For example, few ångström resolution imaging was obtained from large crystalline metal-organic framework specimens containing also heavy metals [13]. In other cases [12], the authors increased the spatial resolution in the HRTEM imaging of polymers, from 2.1 nm to 0.36 nm, by a special specimen preparation procedure that adds oxidants to the pristine materials.

The need to image at high resolution small proteins, difficult to be crystallized for typical X-ray protein crystallography methods [20,21], was tackled by Cryo-EM, which was acknowledged with the Nobel Prize in chemistry in 2017 [22]. The method does not image but reconstructs, at typical resolution so far between about 4Å and 2Å, the three-dimensional structure of individual macromolecules, assumed to be in identical or similar conformation, in specimens vitrified at cryogenic temperature [23,24]. Cryo-EM requires the acquisition of numerous two-dimensional low-dose TEM images of the macromolecules in different projections, which are then computationally combined to finally provide a three-dimensional reconstruction that can be interpreted as an electron density map. There are some limitations in the size of the protein particles that can be reconstructed, which should not exceed about 35 kDa, due mainly to the fact that the molecules are embedded in amorphous ice. Additionally, the models derived by Cryo-EM need to be validated and large workgroups are committed to this aim, especially in the near-atomic resolution range [24]. A

 doi:10.20944/preprints202404.1348.v1

comprehensive review on limits, performances and ultimate perspectives of cryo-EM was provided by R. M. Glaeser [25].

Here is shown that sub-ångström high-contrast direct imaging of pristine soft matter at room temperature is, conversely, possible by a recent experimental method that uses a combination of in-line electron holography and low-dose HRTEM, and hence named HoloTEM. The main aim here is not to solve a specific material problem, but to make evident that soft matter can be imaged at the ultimate instrumental resolution by following a procedure capable to overcome the experimental limitations encountered when imaging soft matter by HRTEM. The experiments were performed on advanced field emission gun spherical aberration corrected TEM [26], equipped with high-speed, high sensitivity direct detection cameras. As case study we tackled a crystalline polymer-based material, highly sensitive to the radiation damage. The approach is effective even on single nanometric pristine crystalline particles and the relevant experimental atomic resolution images can be quantitatively simulated, opening new perspectives in the study of radiation sensitive materials.

In–line electron holography was established in the forties of the last century by Gabor [27] to overcome the spatial resolution limitations in TEM due to electron lens aberration. Since then, electron holography was used for several different aims in electron microscopy (see [28] and references therein). HoloTEM method uses extremely low-dose-rate real time in-line holograms for the specimen survey, capable to detect crystalline particles suitably oriented for HRTEM imaging. Once the particle has been found, the hologram enables to safely check when the specimen drift stops. Then, the hologram is used for tuning the electron optical conditions by fine focusing the objective lens and spreading the illumination conditions on the area of interest to minimize the electron dose, while achieving the best illumination condition for a high-coherent electron-wave ideal for HRTEM imaging. All these steps can be made while delivering a total dose well below the structural damage threshold [28]. As evidenced in the following, the possibility to use the low-dose hologram to evaluate in advance the diffracting conditions of the particles, enables to use doses of electrons for HRTEM imaging higher than the ones theoretically predicted [28]. The final low-dose HRTEM image is hence acquired by using state-of-the-art high-speed high-sensitivity direct detection imaging cameras that enable to grab series of hundreds of low-dose HRTEM images to check offline the possible appearance of structural damage as a function of the density of electrons delivered to the specimen. The result of the experiments is a high signal-to-noise ratio HRTEM image, which is the sum of individual damage-free images, whose spatial resolution, in our experiments, depends on the equipment set-up and hence could reach sub-ångström performances on state-of-the-art TEM instruments. It is worthwhile to remark here, that HoloTEM enables to perform room temperature atomic resolution imaging on pristine organic materials without any staining or special specimen preparation procedures and can be applied not only to large specimens [13] but also to small individual not identical nanoparticles, with their own crystal structure and polymorph statistical distribution within the material [29], enabling to perform on soft matter quantitative HRTEM experiments as those so far possible only on radiation robust inorganic nanomaterials.

2. Materials and Methods

In this study two different polymers based on polyethylene glycol (PEG), a ubiquitous polymer with applications in a variety of fields like medicine, biology, chemistry, were used in combination with caffeine (caf) and fluoroanthranilic acid (ana), as precursors for cocrystal synthesis in a polymer-assisted grinding (POLAG) process [30]. The discovery of a cocrystal between caf, 6-fluoroanthranilic acid (6Fana) and PEG-DME 1000 in our previous study prompted us to perform a cocrystal screen using other fluorinated anthranilic acid derivatives, which led to the discovery of a new cocrystal composed of caf, 5Fana and PEG-DME 1000 (CAPeg). The new polymer-based cocrystals were prepared mechanochemically in absence of liquid additives (see §1 in the Supplementary Information). During the screening stage, we also observed that the replacement of PEG-DME with PEG-PPG produces an isostructural solid (CAP). The solid products obtained mechanochemically were preliminarily characterized using powder X-ray diffraction and differential scanning calorimetry.

 doi:10.20944/preprints202404.1348.v1

Powder X-ray diffraction (PXRD) patterns of the mechanochemically prepared solids were collected at room temperature using a Bruker D2 Phaser diffractometer (Bruker, Manheim, Germany) equipped with a low power (300 W) X-ray source (30 kV at 10 mA) generating Ni-filtered CuK_a radiation (λ=1.54184 Å), and a SSD160-2 detector. The steel sample holder has an internal volume of 300 μl³, which can be reduced to 100 μl³ through a home-made cylindrical gearbox in polyvinylidene fluoride. The measurement parameters were: 2θ angles from 5° to 35°, 2θ steps of 0.02°, counting time of 0.6 s per step. The measurements are reported in Figure S1, Figure S2 and Figure S3 and are compared with the simulated diffractograms (see Supplementary Information §2).

Differential scanning calorimetric (DSC) measurements were performed on a *Mettler Toledo DSC 3* instrument. Approximately 3 mg of each solid were weighed in a 40 μL alumina pan and covered with an alumina lid. The samples were heated under the flow of dry nitrogen gas from 30 °C to 250 °C, with a heating rate of 10 °C min^{-1}. The DSC curves were processed using the *Mettler STAR^e* data evaluation software (version 16.40). The relevant measurements are reported in Figure S4 of the Supplementary Information.

Single crystals of the CAPeg were obtained through recrystallization from the melt (see §2 in the Supplementary Information) and studied at the XRD1 beamline at Elettra Synchrotron to determine the material crystallographic structure (see §3 in the Supplementary Information). Standard low-dose TEM/STEM experiments performed on pristine materials at room temperature immediately resulted in the disruption of the polymeric matter, already during the survey necessary to find the particles of interest. This evidence urged the use of a different approach for TEM investigation. As demonstrated here, HoloTEM enabled to achieve ultimate resolution in low-dose HRTEM experiments while avoiding specimen damage. Details on the TEM specimen preparation and of the state-of-the-art equipment used for the HoloTEM experiments are reported in §4 and §5 of the Supplementary Information, respectively.

In-line electron holography (see Scheme 1) enabled to detect with high contrast the nanoparticles of the polymeric matter sustained on a standard TEM Cu grid covered with a thin carbon film, while delivering an extremely small density of electrons: ρ≈0.1e$^-$/Å².

The ray diagram in the Scheme 1 points that, by tuning the electron optics, an in-line hologram (magnified ten times in Scheme 1 for reader convenience) is formed in the back focal plane of the objective lens, where the interference between the reference wave and the wave diffused by the specimen makes the nanoparticle sharply visible despite the low-dose, the latter being insufficient for standard multibeam imaging live survey as formed on the image plane (see Scheme 1). The experimental hologram and the multibeam image shown in the Scheme 1 are representative of what is actually seen by the scientist, in real time at density rate of current ≤ 1.2e$^-$/s Å², during the survey to find the area of interest on a standard Cu (C-coated) grid, by live low-dose in-line holography or by standard live low-dose imaging, respectively.

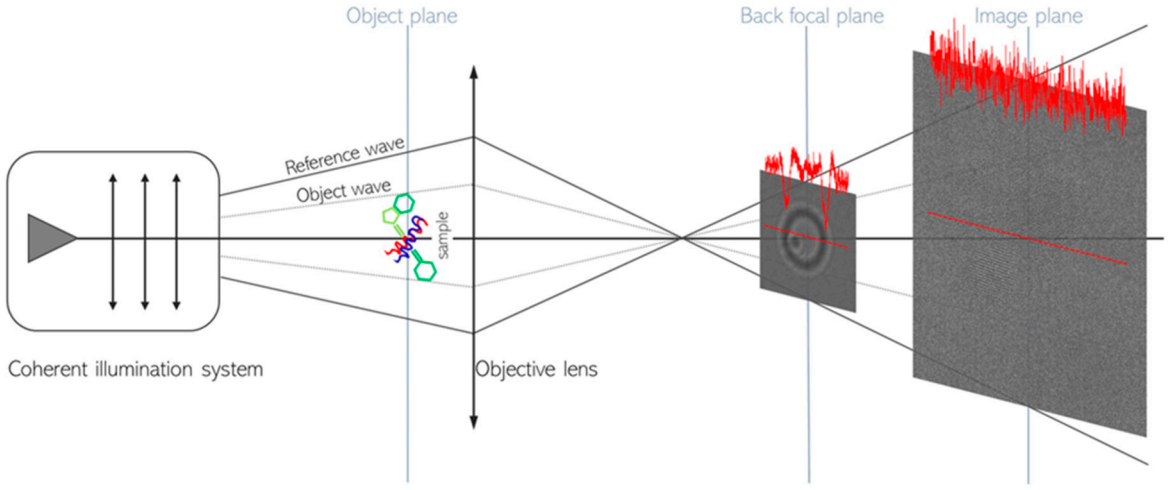

Scheme 1. HoloTEM experiment layout: on the left part the high coherence illumination source, the illumination lenses, the specimen position within the illuminating electron wave field and the

 doi:10.20944/preprints202404.1348.v1

objective lens are sketched. On the right part the experimental live low-dose hologram (magnified ten times) and the relevant live low-dose HRTEM image are reported to show what is live-observed during the survey to find the particles on the TEM grid. The one order of magnitude contrast difference between the captured live hologram and the relevant captured live multibeam image is quantified by the intensity profile measured across the particle.

The nanoparticles imaged in the Scheme 1 are cocrystals made of caffein, 5-fluoranthranilic acid and polyethylene-polypropylene copolymer (CAP) that were dispersed on the TEM grid (see below and Supplementary Information §4.). The peculiarities of the HoloTEM method for the specimen survey are evident by comparing the in-line hologram and the relevant TEM image in terms of contrast (see red lines intensity profiles on the hologram and on the image) and field of view. The high contrast of the hologram (about 33%) compared to the faint contrast of the conventional multibeam image (less than 4%), points that, according to the Rose's criterion [31], the particles are practically invisible in a standard imaging survey at low-dose, whereas the holograms ensure an immediate and good particle detection (see also Figure S7 in the Supplementary Information). Furthermore, the field of view of the in-line hologram is thousand times wider than the one of the standard images, enabling a realistic search for the particles of interest across a standard TEM specimen that can contain particles of different sizes and different kinds (see §4 in the Supplementary Information). It is worth to further underline that the HRTEM image in Scheme 1 is representative of the conditions of low-dose live particle-search and not of the HRTEM image that can be acquired by HoloTEM procedure. The difference between the two conditions is immediately evident comparing the low contrast HRTEM in the Scheme 1 with the high contrast HRTEM image on the same particle as shown in Figure S7 of the Supplementary Information. The latter has a contrast that enables sub-Å resolution imaging on the equipment like the one used in this work, as can be derived from the relationship between the fluence, the contrast and the attainable resolution according to the Rose criterion [14,28,30]. The data in the Scheme 1 also represent a synopsis of a HoloTEM experiment: using the real time hologram at low-dose and low-dose-rate, the particle can be located choosing those well oriented for HRTEM imaging. The electron optics can be there optimized, as detailed below, and the specimen holder drift checked, until it stops. Hence, the set-up can be rapidly switched to HRTEM mode acquiring 100-200 images on the same area with an exposure time, for each image, on the millisecond scale (see §5 in the Supplementary Information). This procedure ensures a safe density of current $\rho < 2$ $e^-/Å^2$ for each image and enables full control over the appearance, and the eventual development, of radiation damage (see Figure S6 in the Supplementary Information). Finally, the images can be summed to obtain a final HRTEM micrograph with a good signal-to-noise ratio that can be numerically simulated to quantify the specimen properties (see §5 and §6 in the Supplementary Information).

The crystallographic structure of the material derived by the synchrotron XRD experiments was used in the quantitative simulations of the atomic resolution imaging experiments here. Further details and examples are reported in the Supplementary Information file at §5 and §6. HoloTEM combines the use of in-line holograms with low-dose HRTEM, resulting in an experimental procedure that enables an extremely accurate control of the equipment illumination system, and an effective way to detect the particle of interest, with diffraction conditions suitable for HRTEM imaging, on a standard unstained TEM specimen, while monitoring the possible radiation damage [28]. It should be remarked that, in a conventional HRTEM experiment for single nanoparticle imaging, the dose delivered during the exposure time for image acquisition is only a fraction of the problem [13]. The greater issue is due to the irradiation to which the specimen is exposed while finding the particles of interest on the TEM grid. At the values of ρ necessary not to damage the specimen it is impossible, in a standard imaging, to distinguish any organic unstained particle due to the low scattering power of light elements [18, 28] (see Scheme 1). Further specimen irradiation occurs while waiting until the mechanical inertia of the specimen holder ends, during particle orientation and during the fine tuning of electron optics on the region of interest. All these operations are mandatory before imaging acquisition for quantitative analysis and can be properly performed by HoloTEM [16].

 doi:10.20944/preprints202404.1348.v1

3. Results and Discussion

The results reported in the following show representative HoloTEM experiments on polymer-based specimens that provide the evidence that sub-ångström HRTEM images on soft matter can be obtained with an unprecedent confidence on all the experimental parameters necessary for quantitative HRTEM imaging of single pristine nanoparticles and on the dose reaching the specimen and on its effect.

Figure 1 shows the raw HRTEM image of a CAP particle together with the relevant hologram (see the inset) and demonstrates that high quality low-dose HRTEM images can be obtained on pristine polymeric material.

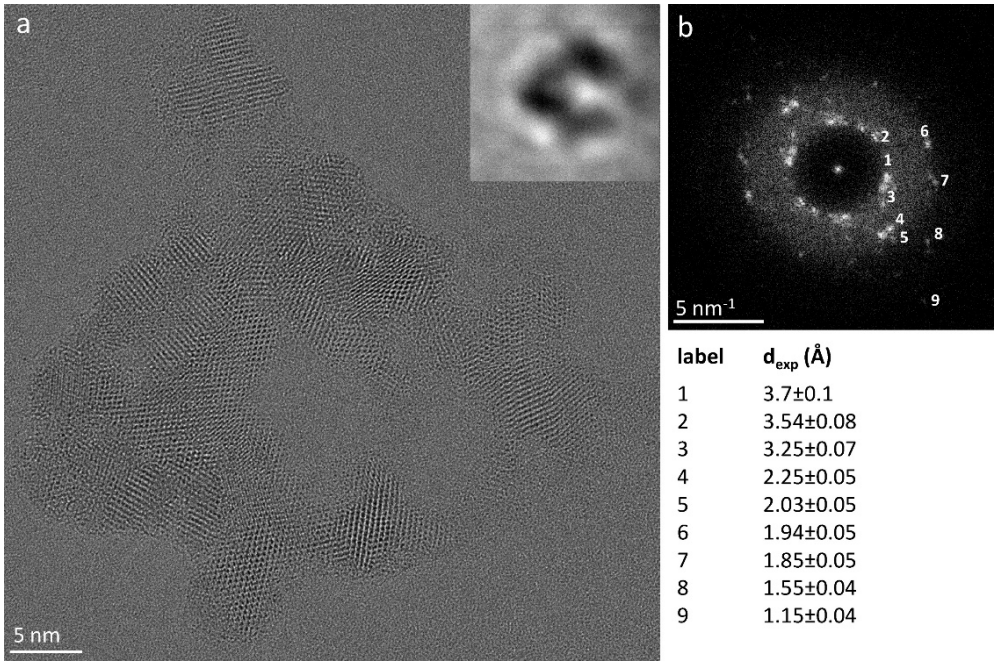

label	d_{exp} (Å)
1	3.7±0.1
2	3.54±0.08
3	3.25±0.07
4	2.25±0.05
5	2.03±0.05
6	1.94±0.05
7	1.85±0.05
8	1.55±0.04
9	1.15±0.04

Figure 1. HRTEM image of a cluster of crystalline pristine polymeric nanoparticles: (**a**) HRTEM image, with the relevant hologram in the inset, of a cluster made of CAP nanoparticles. (**b**) Diffractogram of (**a**) and list of the lattice spacing measured within each nanoparticle.

The HRTEM image is the sum of 100 images, each image received a ρ~7e^-/Å^2 without showing detectable damage (see Materials and Methods and the Supplementary Information §6). The experiments point that monitoring the possible damage by HoloTEM procedures enables to maximize the electron dose delivered to the specimen before the onset for structural damage. In fact, the expected dose limits [17] can be properly relaxed when the particle is well oriented along a zone axis, a very low-dose-rate is used [1,30,32,33], protective layers of hydrocarbon contaminants are formed [14,33,34], the illumination spread is maximized and the possible damage development is monitored by multiple low-dose image acquisition (see §6, Figure S6 in the Supplementary Information). During the experiments we noticed that the particle disruption is strongly related to its diffraction conditions. A reason that can contribute to this behavior is because, when the particle is well oriented along a zone axis, the scattering is eminently elastic [35] whereas the damage to the crystal structure is mainly due to inelastic scattering [36], the latter being reduced in electron channeling conditions [37]. Leaving unchanged all the other experimental parameters, this leads to a higher robustness to the damage of well oriented particles with respect to particles not oriented for high channeling conditions (see Supplementary Information §6.6 and Figure S10) even if, for the knowledge up to now, the effect of the channeling alone could not explain quantitively the observed phenomenon. To our knowledge, the role of the particle diffraction conditions was not considered so far when calculating the maximum resolution reachable in TEM imaging before damage [14,28]. Hence, the values reported in literature represent the minimum in the electron dose deliverable to a particle irrespective to its diffraction condition. On the contrary, higher values of dose could be safely

 doi:10.20944/preprints202404.1348.v1

delivered when the particle is well oriented along a zone axis, enabling to achieve higher spatial resolution. Low-dose live in-line holograms enable a conscious choice of the particle orientation during the specimen survey. A systematic study on tailored specimens would be necessary to quantify this aspect, but the results in Figure S10 evidence how the delivered dose to a well oriented crystalline polymer particle can be at least two orders of magnitude higher than previously believed. Indeed, for reader convenience, we report in the Supplementary Information, §6.6 and Figure S10, an example of an irradiation experiment on a pristine unstained particle of pure PEG where density of electrons up to at least $10^2 e^-/Å^2$ does not cause evidence of particle damage, and a density of electrons of $85.4 \times 10^3 e^-/Å^2$ is necessary to make most of the particle volume amorphous.

The high signal-to-noise ratio of the experimental HRTEM image obtained by HoloTEM, which is at a first glance from figure 1 comparable to the one achievable on inorganic matter, enables to quantify the material properties by measuring the lattice spacing of each nanoparticle forming a cluster, as shown by the diffractogram on Figure 1b and by the relevant list of the measured lattice spacing. It is worth to note that the cluster shape immediately highlights the tendency of polymer-based cocrystals to form closed structures while maintaining the mechanical flexibility, as already observed in our previous studies [30].

Figure 2a is the raw HRTEM image of a 12nm × 18nm thin nanoparticle of CAPeg cocrystal, isostructural to CAP cocrystal (see Materials and Methods and §1, §2 and §3 in the Supplementary Information). The micrograph is the sum of 100 images. Each image has been exposed to a density of electrons $\rho = 2 e^-/Å^2$. The structure of CAPeg, as derived by synchrotron XRD experiments (see Figure 2c below, §2 and §3 in the Supplementary Information and the associated content .cif structural file), was used to simulate the HRTEM results (see Figure 2b and the inset marked in pale blue in Figure 2a) by JEMS computer program using multislice full dynamical calculations [38]. The orientation of the particle with respect to the microscope optical axis was addressed by comparing the experimental diffractograms with those calculated by JEMS using the structural .cif file obtained by XRD experiments (see .cif file supplied in the Supplementary Information). The simulation marked by the pale blue square within the raw experimental HRTEM image is calculated for the [3, 6, $\bar{4}$] zone axis of the triclinic crystal cell and well matches the experimental contrast. In Figure 2, the experimental diffractogram (d), the simulated diffraction pattern (e), and the measured (d_{exp}) and calculated (d_{theo}) lattice spacing are also reported. The HRTEM image and the relevant diffractogram evidence that the particle is a crystalline monodomain. The structure and the size of these nanoparticles are directly accessed by HoloTEM atomic resolution imaging experiments and are related to the synthesis conditions [30] demonstrating as HRTEM imaging and relevant simulations can be performed on polymeric material overcoming the sensitivity to the radiation damage.

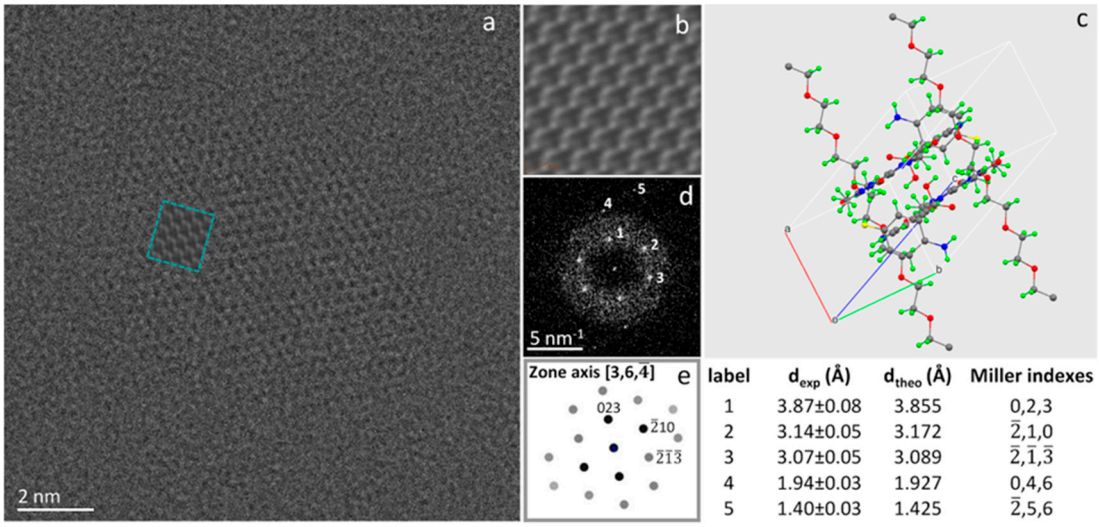

label	d_{exp} (Å)	d_{theo} (Å)	Miller indexes
1	3.87±0.08	3.855	0,2,3
2	3.14±0.05	3.172	$\bar{2}$,1,0
3	3.07±0.05	3.089	$\bar{2},\bar{1},\bar{3}$
4	1.94±0.03	1.927	0,4,6
5	1.40±0.03	1.425	$\bar{2}$,5,6

Figure 2. Atomic resolution quantitative imaging experiment on a single CAPeg nanoparticle: a) HRTEM image in the [3, 6, $\bar{4}$] zone axis of a polymer-based cocrystal CAPeg particle; in the pale blue inset the relevant multislice simulation is reported; b) magnified view of the HRTEM contrast simulation; c) crystal structure as derived from single crystal XRD experiments and displayed by

 doi:10.20944/preprints202404.1348.v1

using computer program Mercury [39]; the unit cell is viewed along the [3, 6, $\bar{4}$] zone axis as in the experimental image. The sticks and balls represent by different colours bonding of the chemical species: hydrogen = green, fluorine = yellow, oxygen = red, carbon = grey and nitrogen = blue. d) experimental diffractogram, e) simulated diffraction pattern in the [3, 6, $\bar{4}$] zone axis and experimental (d_{exp}) and calculated (d_{theo}) spacing along with the relevant Miller indexes.

Moreover, further subtle structural features at sub-Å spatial resolution can be quantitatively achieved on the specimen, as shown in Figure 3. Figure 3a is a raw HRTEM image showing part of a large thin foil of CAPeg in the [10, 3, 2] zone axis. The experimental image is the sum of 100 frames. Each frame has been exposed to ρ=0.8e^-/Å^2 to check offline for the possible damage (see §6.1 and Figure S6 in the Supplementary Information). The analysis of Figure 3 is helpful for understanding some subtle peculiarities of the cocrystal system studied. Indeed, the HRTEM images of CAPeg have some uncommon features, mostly evident on relatively large foils of some hundreds of nm in size, which could be related to the typical flexibility of polymers, well known on a macroscopic scale, and here directly evidenced on atomic scale. In fact, we observed small in plane and out of plane tilts making the lattice fringes spacing slightly different from place to place. Some areas show compressive strain and some other tensile; the distortion is hardly visible without comparing the experimental image with a reference. (see Supplementary Information §6.5 and Figure S9). Interestingly, such local strain does not generate visible extended defects and cracks, as it would be in other more rigid solids [40]. These results demonstrate that the study of crystalline polymeric materials at atomic resolution allowed by HoloTEM, would very likely require the modification of some paradigms we are used to, including the concept of rigidity often associated to the concept of crystal where, when the crystal symmetry is broken by stress, it results in regions bounded by extended defects [40].

Figure 3b shows the diffractogram of the HRTEM image in (a). The intensities are distributed on rings, and their anisotropic distribution on the rings indicate that the foil consists of grains with the same orientation in the direction normal to the foil and textured in the plane of the foil [41]. Some of the most visible spacing have been numbered from 1 to 11 in the diffractogram in Figure 3b and the relevant experimental values are reported together with the Miller's indexes and spacing calculated by JEMS. The blue square in (a) marks an individual grain shown at high magnification in Figure 3c where fine structural details can be distinguished but, to be quantified and rationalized, need the comparison with the pertinent image simulation [42]. The relevant diffractogram is shown in Figure 3d, where the (0, -2, 3) and (1, -2, -2) reflections are marked. The relevant vectors are the base vectors for the plane perpendicular to the [10, 3, 2] direction, which is parallel to the one of the primary beam. The comparison between experimental and simulated diffractogram is reported in Figure S8 of the Supplementary Information, where the experimental pattern is superimposed to the simulated one for ease of comparison. In the diffractogram, the reflections (4, -6, -11) and (3, -10, 0) are also marked by circles as they correspond to two distinguished sub-Å spacing, pointing that the highest spatial resolution enabled by the equipment can be here reached on soft-matter (see Supplementary Information §5) despite its sensitivity to the radiation damage. It is worthwhile to remark, that dynamical scattering could result in non-linear effects producing sub-Å intensities in the diffractogram that could not correspond to real structural features within the particles, and hence not contributing to the image resolution [43,44]. A way to disclose this subtle point, is to simulate the HRTEM image and to identify the structural features originating the measured sub-Å spacing. In the experimental image in Figure 3c this task is a bit complicated by the complexity of the atom arrangement within the unit cell, by the distortion of the bonds and by some thickness variation within the observed area. Indeed, the fitting image simulation superimposed in the top-left part of Figure 3c has been calculated for a thickness of 27 nm, whereas the area about in the centre of the image has been simulated for a thickness of 18 nm. The details of the image simulation are reported in the Supplementary Information §6.4. Figure 3e is the crystal cell of CAPeg as calculated from the synchrotron x-ray diffraction measurements and shown in the same orientation [10, 3, 2] of the experimental HRTEM image. The grey rectangle marks part of the atomic configuration of the CAPeg crystal cell shown magnified in the lower-right part of the figure. The display has been obtained by Mercury software [39]. The atoms in the cell are shown by different colours: H atoms are green, F

 doi:10.20944/preprints202404.1348.v1

atoms are yellow, O atoms are red, C atoms are grey and N atoms are blue. The pale-red lines in Figure 3e are the traces of the planes (3, -10, 0) and (4, -6, -11). These lattice planes are those generating the intensities marked in the experimental diffractogram and corresponding to the measured spacing of 85 pm and 93 pm respectively. In the lower-right part of Figure 3e these spacing are marked by the dashed grey and red lines respectively. This result evidences that the spacing at 93 pm is due mainly to the marked carbon-oxygen dumbell, whereas the spacing at 85 pm is due mainly to marked carbon-carbon atoms. The same atomic configuration has been superimposed for reader convenience to the image simulation in Figure 3c to underline their structural correspondence. It should be marked that not only the distances but also the angles formed by the dumbell in the (4, -6, -11) and (3, -10, 0) planes are coherent between experiments and simulations, as shown in Figure 3, pointing the structural correspondence and ruling out that the sub-Å spacing could be due to a non-linear effect in the HRTEM image.

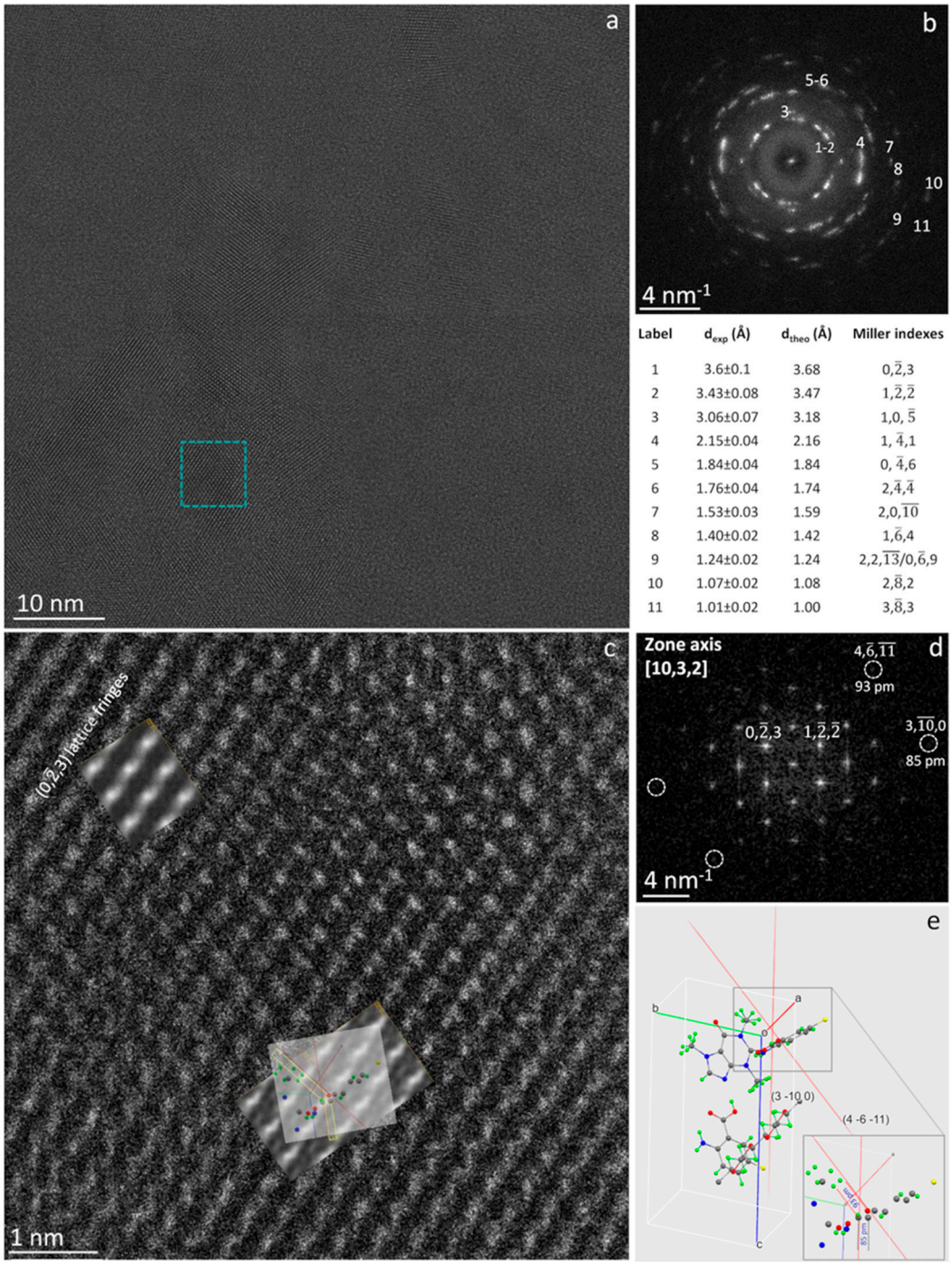

Label	d_{exp} (Å)	d_{theo} (Å)	Miller indexes
1	3.6±0.1	3.68	$0,\bar{2},3$
2	3.43±0.08	3.47	$1,\bar{2},\bar{2}$
3	3.06±0.07	3.18	$1,0,\bar{5}$
4	2.15±0.04	2.16	$1,\bar{4},1$
5	1.84±0.04	1.84	$0,\bar{4},6$
6	1.76±0.04	1.74	$2,\bar{4},\bar{4}$
7	1.53±0.03	1.59	$2,0,\overline{10}$
8	1.40±0.02	1.42	$1,\bar{6},4$
9	1.24±0.02	1.24	$2,2,\overline{13}/0,\bar{6},9$
10	1.07±0.02	1.08	$2,\bar{8},2$
11	1.01±0.02	1.00	$3,\bar{8},3$

Figure 3. Sub-ångström imaging experiment on a CAPeg thin foil: a) Raw HRTEM image showing part of a large foil of CAPeg in the [10, 3, 2] zone axis, along with, in b), the relevant diffractogram

 doi:10.20944/preprints202404.1348.v1

and experimental (d_{exp}) and calculated (d_{theo}) spacing together with the corresponding Miller's indexes. The blue square in a) marks the area shown at higher magnification in c). In c) two image simulations are superimposed to the HRTEM raw image, fitting the experimental contrast for two different thickness values: 18 nm in the upper left part of c) and 27 nm in the central-lower part of c). d) Is the diffractogram of c) evidencing two basic vectors for the plane perpendicular to the [10, 3, 2] direction, and the reflections (4, -6, -11) at 93 pm and (3, 10, 0) at 85 pm. e) Cell of CAPeg seen along the [10, 3, 2] zone axis displayed by Mercury software [39], highlighting the traces of the planes (4, -6, -11) and (3, -10, 0) and the relevant oxygen-carbon and carbon-carbon dumbell, respectively. The grey rectangle marks the atomic configuration of CAPeg seen magnified in the lower-right part of e), where the two sub-Å dumbell are underlined by grey and red dashed lines. This atomic configuration is then also shown superimposed to the HRTEM image and simulations in the central-lower part of c).

4. Conclusions

HoloTEM experiments demonstrate that pristine polymeric nanomaterials can be imaged at sub-ångström resolution at room temperature. So far it was believed not possible to directly study soft matter at this degree of spatial resolution and accuracy and to compare quantitatively the experimental atomic resolution image to the geometry of the simulated one to understand subtle properties of these materials. Here, the direct comparison between experiments and simulations by using full dynamical calculations is enabled by the relatively high-signal-to-noise ratio of the experimental images, despite the low scattering power of the organic materials, and it is made possible by the accurate control of both electron optical and particle scattering conditions achievable by the hologram at a dose below the threshold for structural damage. To our knowledge direct comparison between atomic resolution HRTEM experiments and image simulations was never reported so far in the literature. Furthermore, the experiments point that, the well-controlled imaging conditions allowed by HoloTEM, the possibility to recognize in advance by the holograms the channeling conditions suitable for HRTEM, the use of a low-dose-rate of electrons, coupled with the formation of very thin protective hydrocarbon layer, enable the use of a total density of electrons higher than the one previously believed possible for imaging soft matter [14,28]. Direct imaging at sub-ångström resolution opens new scenarios for the understanding of the properties of soft matter and, as recently theoretically predicted, it is key for the application of in-line electron holography to atomic resolution three-dimensional shape reconstruction of crystalline soft matter nanoparticle from a single projection [45]. In case of CryoEM, the accuracy of HRTEM imaging and relevant simulations enabled by HoloTEM can be used to improve the knowledge and the constraint necessary for accurate and reliable CryoEM reconstruction. Among other aspects that HoloTEM opens in the study of soft-matter, there is the development that can be foreseen from the quantitative understanding of the phase shift information contained in the holograms [46].

Supplementary Materials: The following supporting information can be downloaded at the website of this paper posted on Preprints.org. CIF file for the structure of CAPeg solved by Synchrotron X-Ray diffraction on single crystal. - .pdf file of the Platon report on the structural .CIF file. - .DM4 files of the image series for figure S6. - Supplementary Information file containing the following paragraphs, figures, and tables: §1. Mechanochemical synthesis of polymer based cocrystals. §2. Preparation of a single crystal of CAPeg. §3. Single crystals X-ray diffraction studies. §4. TEM sample preparation for HoloTEM. §5. Experimental HoloTEM. §6. Additional on HoloTEM experiments, HRTEM image Simulations and EDXS experimental results. Figure S1: XRD measurements. Figure S2: XRD measurements. Figure S3: XRD measurements. Figure S4: DSC measurements. Figure S5: Structure determination. Figure S6: Example of multiple Low-dose HRTEM image series. Figure S7: High spatial resolution experiment on CAP multidomain nanoparticle. Figure S8: Simulated and experimental diffraction pattern. Figure S9: Strain in CAPeg foils. Figure S10: Radiation damage in pure PEG particle. Diffraction conditions heavily influence the particle robustness to electron irradiation. Figure S11: EDXS Spectra on CAPeg particles. Table S1: Structural determination and refinement parameters of CAPeg.

Author Contributions: **E. C.** Developed the HoloTEM method. **E.C., L.E.C., A. T.** did the HoloTEM experiments. **E.C. and A. T.** analyzed the data and did the image simulation by JEMS. **E.C and L.E.C** prepared the TEM specimen. **J.J.C.G** coordinated the work at the Electron Microscopy facility at the University of Cadiz. **D. H**. made the cocrystalline polymers, **M.P.** did the XRD measurements at the synchrotron deriving the crystal

structure, **DKB** further refined the crystal structure. All authors discussed the results and contributed to the final manuscript.

Funding: This research was funded by the project PID2020-113006-RB-I00 funded by MCIN/AEI/ 10.13039/50110001103.

Data Availability Statement: experimental data other than those published and included in the supplementary files can be provided on motivated request to the corresponding author.

Acknowledgments: E.C. would like to thank the University of Cadiz for the invited visiting professorship.

Conflicts of Interest: The authors declare no conflicts of interest.

References

1. Hirsch P.B. TEM in materials science-past, present and future. *J. Microsc.* **1989**, *155 (3)*, 361-371.
2. Williams D.B.; Carter C.B. *Transmission Electron Microscopy: A Textbook for Materials Science*, 2nd ed.; Springer Science + Business Media, L.L.C New York, 2009.
3. Carlino E. *Advances in Transmission Electron Microscopy for the study of the soft and hard matter*, Special Issue of Materials, MDPI St. Alban-Anlage 66 ISBN 978-3-0365-3213-4, 2022.
4. Feynman R.P. There is plenty of room at the bottom. *Eng. Sci.* **1960**, *23*, 22-36.
5. Haider M.; Hartel P.; Müller H.; Uhlemann S.; Zach J. Current and future aberration correctors for the improvement of resolution in electron microscopy. *Philos. Trans. R. Soc. A* **2009**, *367*, 3665–3682.
6. De Caro L.; Carlino E.; Caputo G.; Cozzoli P.D.; Giannini C. Electron diffractive imaging of oxygen atoms in nanocrystals at sub-ångström resolution. *Nat. Nanotechnol.* **2010**, *5*, 360–365.
7. Hawkes P.W.; Kasper E. *Wave optics*: Vol. 3 London: Academic Press Inc., 1994.
8. Haider M.; Rose H.; Uhlemann S.; Schwan E.; Kabius B.; Urban K. A spherical-aberration-corrected 200 kV transmission electron microscope. *Ultramicroscopy* **1998**, *75*, 53-60.
9. Sato M.; Orloff J.; A new concept of theoretical resolution of an optical system, comparison with experiment and optimum condition for a point source. *Ultramicroscopy* **1992**, *41*, 181-192.
10. Tate M.W. et al., High Dynamic Range Pixel Array Detector for Scanning Transmission Electron Microscopy. *Microsc. Microanal.* **2016**, *22*, 237–249.
11. Claes N.; Asapu R.; Blommaerts N.; Verbruggen S.W.; Lenaerts S.; Bals S. Characterization of silver-polymer core-shell nanoparticles using electron microscopy. *Nanoscale* **2018**, *10*, 9186-9191.
12. B. Kuei, E.D. Gomez, Pushing the limits of high-resolution polymer microscopy using antioxidants. *Nat. Commun.* **2021**, *12*, 153, https://doi.org/10.1038/s41467-020-20363-1.
13. Zhang D.; Zhu Y.; Liu L.; Ying X.; Hsiung C.; Sougrat R.; Li K.; Han Y. Atomic-resolution transmission electron microscopy of electron beam–sensitive crystalline materials. *Science* **2018**, *359*, 675–679.
14. Egerton R.F.; Li P.; Malac M.; Radiation damage in the TEM and SEM. *Micron* **2004**, *35*, 99–409.
15. Egerton R.F. Control of radiation damage in the TEM. *Ultramicroscopy* **2013**, *127*, 100–108.
16. Spence J.C.H. Experimental High-Resolution Electron Microscopy, 2nd ed., Oxford University Press Inc.: New York, NY, USA, ISBN 0-19-505405-9, 1988.
17. Henderson R. Cryo-protection of protein crystals against radiation damage in electron and X-ray diffractions. *Proceedings of Royal Society of London B* **1990**, *241*, 6–8.
18. Libera M.L.; Egerton R.F. Advances in the transmission electron microscopy of polymers. *Polym. Rev.* **2010**, *50*, 321-339.
19. Van Tendeloo G.; Bals S.; Van Aert S.; Verbeeck J.; Van Dyck D. Advanced electron microscopy for advanced materials. *Adv. Mater.* **2012**, *24* (42) 5655-5675.
20. Chapman H.N.; Fromme P.; Barty A.; White T.A.; Kirian R.A.; Aquila A.; Hunter M.S.; Schulz J.; De Ponte D.P.; Weierstall U.; et al., Femtosecond X-ray protein nanocrystallography. *Nature* **2011**, *470*, 73–77.
21. Kermani A.A. A guide to membrane protein X-ray crystallography. *FEBS J.* **2020**, *288*, 5788-5804, doi: https://doi.org/10.1111/febs.15676.
22. https://www.nobelprize.org/prizes/chemistry/2017/press-release/.
23. Cheng Y. Single-particle Cryo-EM at crystallographic resolution. *Cell* **2015**, *161*, 450-457.
24. Lawson C. L. et al. Cryo-EM model validation recommendations based on the outcomes of the 2019 EMDataResource challenge, *Nat. Methods* **2021**, *18*, 156-164.
25. Glaeser R. M. How Good Can Single-Particle Cryo-EM Become? What Remains Before It Approaches Its Physical Limits? *Annu. Rev. Biophys.* **2019**, *48*, 45–61. Doi: /10.1146/annurev-biophys-070317-032828
26. P.W. Hawkes, The correction of electron lens aberration. *Ultramicroscopy* **2015**, *156*, A1–A64.
27. Gabor D. A new microscopic principle. Nature **1948**, *161*, 777–778.
28. Carlino E. In-line holography in transmission electron microscopy for the atomic resolution imaging of single particle of radiation sensitive matter. *Materials* **2020**, *13* (6), 1413-1432.
29. Hasa D.; Carlino E.; Jones W.; Polymer-assisted grinding, a versatile method for polymorph control of cocrystallization. *Cryst. Growth Des.* **2016**, *16*, 1772–1779

 doi:10.20944/preprints202404.1348.v1

30. Germann L.S.; Carlino E.; Taurino A.; Voinovich D.; Dinnebier R.E.; Bučar D.K.; Hasa D. Modulating thermal properties of polymers through crystal engineering, *Angew. Chem.–Int. Ed.* **2023**, e202212688, https://doi.org/10.1002/anie.202212688.
31. Rose A. Television pickup tubes and the problem of vision. In *Advances in Electronics*; Marton L. Eds.; Academic Press: New York, NY, USA, 1948, pp.131-166.
32. Nan J.; Spence J.C.H. On the dose-rate threshold of beam damage in TEM. *Ultramicroscopy* **2012**, *113*, 77–82.
33. Egerton R. F.; McLeod R.; Wang F.; Malac M. Basic questions related to electron-induced sputtering in the TEM. *Ultramicroscopy* **2010**, *110*, 991-997.
34. Fryer J.R.; Holland F. The reduction of radiation damage in the electron microscope. *Ultramicroscopy* **1983**, *11*, 67-70.
35. Pennycook S. J.; Jesson D. E. In *Electron Microscopy in Materials Science*; Merli P. G., Vittori-Antisari M., Eds.; World Scientific Pub. ISBN 981-02-0924-X, 1992; pp. 333-362
36. Peet M.J.; Henderson R.; Russo C. J. The energy dependence of contrast and damage in electron cryo-microscopy of biological molecules. *Ultramicroscopy* **2019**, *203*, 125-131.
37. Kirkland E. J. Some effects of electron channeling on electron energy loss spectroscopy, *Ultramicroscopy* **2005**, 102, 199-207.
38. Stadelmann P.A. EMS-a software package for electron diffraction analysis and HREM image simulation in materials science, *Ultramicroscopy* **1987**, *21*, 131–145. JEMS-SaS. Version 4.11531U2022b31 available online: http://www.jems-saas.ch/.
39. https://www.ccdc.cam.ac.uk/
40. Hirth J.P.; Lothe J. *Theory of Dislocations*. Wiley and Sons, 1982.
41. Hirsch P.; Howie A.; Nicholson R.; Pashley D.W.; Whelan M. J. Electron Microscopy of thin crystals, 3rd ed.; R. E. Krieger Publishing Co, Inc, Malabar – Florida, ISBN 0-88275-376-2, 1977.
42. Kisielowski C.; Specht P.; Alloyeau D.; Erni R.; Ramasse Q.; et al. Aberration-corrected Electron Microscopy Imaging for Nanoelectronics Applications. *American Institute of Physics (AIP) Conference Proc.*, 2009, pp.231-240. 10.1063/1.3251226. hal-04276920
43. Van Aert S.; Chen J.H.; Van Dyck D. Linear versus non-linear structural information limit in high-resolution transmission electron microscopy. *Ultramicroscopy* **2010**, *110*, 1404-1410.
44. Kisielowski C.; Hetherington C.J.D.; Wang Y.C.; Kilaas R.; O'Keefe M.A.; Thust A. Imaging columns of light element carbon, nitrogen and oxygen with sub Ångström resolution. *Ultramicroscopy* **2001**, *89*, 243-263.
45. Chen F.-R.; Van Dyck D.; Kisielowski C. In-Line three-dimensional holography of nanocrystalline objects at atomic resolution. *Nat. Comm.* **2016**, *7*, 10603 doi:10.1038/ncomms10603.
46. Lichte H. Electron Holography: phases matter. *Microscopy* **2013**, *62* (Supplement 1), S17-S28.